Intervalence Charge Transfer (IVCT) in Ruthenium Dinuclear and Trinuclear Assemblies Containing the Bridging Ligand HAT {1,4,5,8,9,12-hexaazatriphenylene}

Deanna M. D'Alessandro and F. Richard Keene*[a]

Abstract: The IVCT characteristics of the mixed-valence forms of the dinuclear $[\{Ru(bpy)_2\}_2(\mu\text{-hat})]^{n+}$ and the trinuclear $[\{Ru(bpy)_2\}_3(\mu\text{-hat})]^{n+}$ species {HAT = 1,4,5,8,9,12-hexaazatriphenylene; bpy = 2,2′-bipyridine} show a marked dependence on the nuclearity, and in the trinuclear case on the extent of oxidation. Small differences are also found between the diastereoisomers of the dinuclear complex {*meso* ($\Delta\Lambda$) and *rac* ($\Delta\Delta/\Lambda\Lambda$)}, and between the homochiral (Δ_3/Λ_3) and heterochiral ($\Delta_2\Lambda/\Lambda_2\Delta$) diastereoisomers of the trinuclear case. The strong metal–metal interactions result in unusual spectroscopic and electrochemical properties of the singly-oxidised (+7) and doubly-oxidised (+8) trinuclear mixed-valence species. A qualitative localised bonding description based on the geometrical properties of the $d\pi(Ru^{II/III})$ orbitals is invoked to explain the IVCT behaviour in the di- and trinuclear systems.

Keywords: charge transfer · electrochemistry · mixed-valent compounds · stereochemistry · trinuclear compounds

Introduction

Polymetallic coordination complexes which incorporate two or more transition metal centres have attracted considerable attention over the last decade as part of rapid advances in metallosupramolecular chemistry.[1–5] These complexes display novel electrochemical, photochemical and photophysical properties that may be exploited in molecular-scale devices capable of performing useful light- and/or redox-induced functions, such as molecular recognition and artificial photosynthesis.[6–9] The potential applications of these devices depend on the fundamental intramolecular electron transfer processes that occur between the constituent metal-based chromophores.

The intervalence charge transfer (IVCT) properties of the mixed-valence forms of the polynuclear complexes provide one of the most powerful and sensitive probes of this intermetal electronic interaction.[10,11] To date, IVCT studies have focused predominantly on dinuclear complexes; however, a few reports on higher-nuclearity species have appeared, motivated by the elegant pioneering work of Meyer and coworkers[12] and von Kameke and Taube[13] on pyrazine-bridged molecular chains. The paucity of IVCT studies on tri- and higher nuclearity polymetallic systems is due in part to the presence of multiple, electronically-coupled metal centres which complicate the theoretical analysis, since the electron transfer properties of the assemblies are often not simply a superposition of the characteristics of their component metal-based chromophores.

Three major factors are crucial to extend the IVCT probe to oligonuclear systems: firstly, the effect of increasing the number of electronically-coupled metal centres on the IVCT transitions (specifically, their energy, intensity and bandwidth); secondly, the effect of the relative distances and orientations of the centres; and thirdly, their stereochemical relationship.[14,15] Given the diverse range of metallosupramolecular architectures, these factors underlie the need for a systematic understanding of how the geometry of such systems influences their electron transfer properties.

The bridging ligand HAT (1,4,5,8,9,12-hexaazatriphenylene) represents a particularly attractive basis for polymetallic assemblies as the planar delocalised π-electron system facilitates a strong electronic interaction between the metal centres which are coordinated at the three potential bidentate sites.[14–16] Mono, di- and trinuclear complexes of HAT have been synthesised,[16–28] as well as elaborate three-dimensional assemblies such as molecular squares[29] and mi-

[a] D. M. D'Alessandro, Prof. F. R. Keene
School of Pharmacy and Molecular Sciences
James Cook University, Townsville
Queensland 4811 (Australia)
Fax: (+61) 7-4781-6078
E-mail: richard.keene@jcu.edu.au

Supporting information for this article is available on the WWW under http://www.chemeurj.org/ or from the author: Table S1 with reduction potentials of the di- and trinuclear species.

 DOI: 10.1002/chem.200401038

croporous networks,[19,30,31] all of which have been recognised for their potential applications as biological probes[20,26,27] and as components in novel molecular materials.[32]

We now report the first study on the IVCT properties of the di- and trinuclear systems *meso*(ΔΛ)- and *rac*(ΔΔ/ΛΛ)-$[\{Ru(bpy)_2\}_2(\mu\text{-hat})]^{4+}$, and homochiral ($\Delta_3/\Lambda_3$)- and heterochiral ($\Delta_2\Lambda/\Lambda_2\Delta$)-$[\{Ru(bpy)_2\}_3(\mu\text{-hat})]^{6+}$, shown in Figure 1. The use of these rigid, stereochemically-unambiguous complexes addresses the often neglected stereochemical complexities inherent in such systems, which are known to influence their spectral, electrochemical, photophysical and IVCT properties.[14–16,33–36] The elucidation of the fundamental IVCT properties of these complexes represents a key step in the rational design of higher nuclearity metallosupramolecular systems, in which the intramolecular electron transfer processes may be controlled and ultimately exploited for novel practical applications.

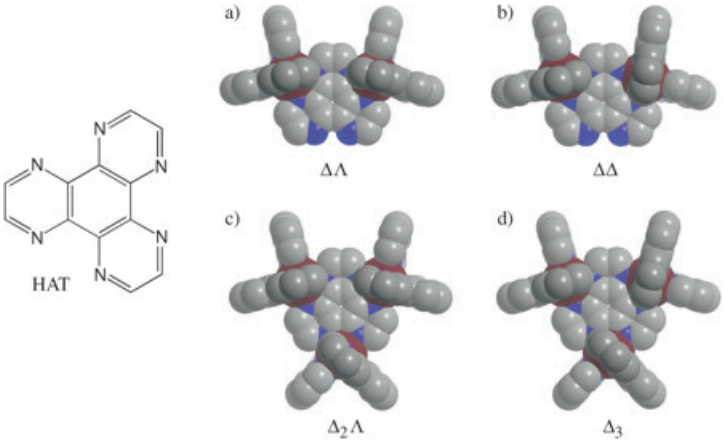

Figure 1. Bridging ligand HAT, and Chem 3D representations of a) the *meso* (ΔΛ) and b) *rac* (ΔΔ) diastereoisomeric forms of $[\{Ru(bpy)_2\}_2(\mu\text{-hat})]^{4+}$, and c) the heterochiral ($\Delta_2\Lambda$) and d) homochiral (Δ_3) diastereoisomeric forms of $[\{Ru(bpy)_2\}_3(\mu\text{-hat})]^{6+}$. Hydrogen atoms are omitted for clarity.

Results and Discussion

Synthesis and stereoisomer separation: The synthetic strategies for the stereoisomerically pure di- {*meso* (ΔΛ) and *rac* (ΔΔ and ΛΛ)} and trinuclear {homochiral (Δ_3 and Λ_3) and heterochiral ($\Delta_2\Lambda$ and $\Lambda_2\Delta$)} systems have been reported previously,[16,17,37] and were based upon a combination of stereoretentive and chromatographic methodologies.[14,15]

Electrochemistry: The electrochemical properties of the stereoisomeric forms[17] of $[\{Ru(bpy)_2\}_2(\mu\text{-hat})]^{n+}$ and $[\{Ru(bpy)_2\}_3(\mu\text{-hat})]^{n+}$ as well as the stereoisomeric mixtures[24,38] of $[\{Ru(bpy)_2\}_2(\mu\text{-hat})]^{4+}$ and $[\{Ru(bpy)_2\}_3(\mu\text{-hat})]^{6+}$ have been reported previously. Electrochemical data obtained by differential pulse voltammetry (in addition to cyclic voltammetry used in the earlier measurements) for the metal-based oxidation processes are given in Table 1.

The di- and trinuclear systems are characterised by two and three reversible one-electron redox processes, respectively, corresponding to successive oxidation of the metal centres. The first two ruthenium-based oxidation processes in Δ_3/Λ_3- and $\Delta_2\Lambda/\Lambda_2\Delta$-$[\{Ru(bpy)_2\}_3(\mu\text{-hat})]^{6+}$ occur at similar potentials to those for their dinuclear congeners. This has been rationalised on the basis that the highest occupied molecular dπ orbital at each ruthenium centre appears relatively unaffected by the additional $\{Ru(bpy)_2\}^{2+}$ moiety in the trinuclear systems.[38,39]

All complexes exhibited multiple reversible ligand-based reductions in the cathodic region (Table S1, Supporting Information). Previous electrochemical studies[38] have established that the first reduction process is localised at the HAT ligand, as a consequence of the lower π* level relative to the peripheral bpy ligands. This was confirmed by the anodic shift of the first reduction process which occurred with an increase in the number of coordinated ruthenium centres, as the increase in nuclearity of the assembly is expected to influence the HAT reduction relatively more than the bpy reductions. On this basis, the second reduction was also attributed to the HAT ligand in the di- and trinuclear complexes, while the third reduction is also based at the bridging HAT moiety in the trinuclear systems.[39]

The potential differences between the successive metal-based oxidation processes (ΔE_{ox}) and comproportionation constants (K_c) have been used previously as semiquantitative criteria to assess the extent of electronic delocalisation and stability of the mixed valence states in dinuclear systems.[40–42] A summary of ΔE_{ox} and the resultant comproportionation constant (K_c[40]) values for the dinuclear and trinuclear complexes is also provided in Table 1.

The separation between the oxidation processes allowed the electrochemical generation of the mono-oxidised +5 mixed-valence forms of the dinuclear complexes, in addition to both the singly- (+7) and doubly-oxidised (+8) mixed-valence forms of the trinuclear complexes.

Electronic spectroscopy: The complete NIR-UV-visible spectral data for the un-oxidised, partially-oxidised and fully-oxidised forms of the di- and trinuclear systems (for the range 3050–30000 cm^{-1}) are given in Table 1. The UV-visible spectra for the diastereoisomeric mixtures of the di- and trinuclear complexes $[\{Ru(bpy)_2\}_2(\mu\text{-hat})]^{4+}$ and $[\{Ru(bpy)_2\}_3(\mu\text{-hat})]^{6+}$ have been described previously,[38,39] and in previous work from our laboratory,[16,17] no significant differences were observed in the spectral properties of the diastereosiomers of either of the un-oxidised systems.

The spectra of the un-oxidised systems in the region from 30000–50000 cm^{-1} are characterised by π→π*(hat) and π→π*(bpy) transitions, where the intensity of the latter are proportional to the number of coordinated $\{Ru(bpy)_2\}^{2+}$ moieties. The UV-visible spectra over the region 15000–30000 cm^{-1} for the un-oxidised +4 forms of the dinuclear systems are characterised by a combination of overlapping $d\pi(Ru^{II})\rightarrow\pi^*(hat)$ and $d\pi(Ru^{II})\rightarrow\pi^*(bpy)$ singlet metal-to-ligand (^{1}MLCT) transitions. The spectra of the un-oxidised

Table 1. UV-visible-NIR spectral[a] and electrochemical[b] data (in mV), and comproportionation constants[c], for the di- and trinuclear complexes. The NIR spectral data are indicated in bold type.

Complex	$n+$	$\nu \pm 10$ [cm^{-1}] ($\varepsilon \pm 0.01$ [$mM^{-1}cm^{-1}$])	E_{ox1}	E_{ox2}	E_{ox3}	$\Delta E_{ox(2-1)}$ (K_c[c])	$\Delta E_{ox(3-2)}$ (K_c[c])
meso-[{Ru(bpy)$_2$}$_2$(μ-hat)]$^{n+}$	4	17910 (15.12)	1168	1392		224(6.26×10^3)	
		21610 (13.27)					
		24250 (16.13)					
	5	**5290 (4.460)**					
		11820 (9.810)					
		22510 (6.340)					
		17260 (9.810)					
	6	11660 (15.83)					
		sh 12750 (8.990)					
		16750 (2.635)					
		24810 (7.010)					
rac-[{Ru(bpy)$_2$}$_2$(μ-hat)]$^{n+}$	4	17930 (17.83)	1156	1380		224(6.26×10^3)	
		21550 (15.85)					
		24190 (18.92)					
	5	**5300 (4.250)**					
		11885 (1.680)					
		13130 (2.700)					
		17360 (10.81)					
	6	11665 (16.62)					
		sh 12990 (9.480)					
heterochiral-[{Ru(bpy)$_2$}$_3$(μ-hat)]$^{n+}$	6	17575 (30.43)	1256	1476	1720	220(5.36×10^3)	244(13.7×10^3)
		19410 (23.92)					
		24545 (16.37)					
		sh 26700 (10.77)					
	7	**4640 (4.180)**					
		5820 (3.265)					
		sh 13070 (2.470)					
		18325 (24.40)					
		sh 25735 (10.93)					
	8	**4910 (2.150)**					
		8190 (4.950)					
		11575 (6.910)					
		13610 (7.650)					
		sh 17650 (14.96)					
		18745 (15.45)					
	9	13495 (18.60)					
		16025 (15.53)					
homochiral-[{Ru(bpy)$_2$}$_3$(μ-hat)]$^{n+}$	6	17620 (35.58)	1256	1486	1726	230(7.91×10^3)	240(11.7×10^3)
		19450 (27.97)					
		24490 (18.74)					
		sh 26830 (12.10)					
	7	**4650 (3.315)**					
		6020 (2.634)					
		sh 7005 (2.380)					
		11070 (1.785)					
		18080 (27.46)					
	8	**4690 (2.990)**					
		7110–8060 (3.285)					
		sh 11170 (4.590)					
		13560 (10.28)					
		sh 17440 (19.79)					
		18310 (21.06)					
	9	13420 (21.06)					
		17600 (14.94)					

[a] Spectroelectrochemical experiments were conducted at −35 °C for the mono-and dinuclear species, and at −15 °C for the trinuclear species, respectively; sh = shoulder of band. [b] All potentials in 0.1 M [(n-C_4H_9)$_4$N]PF_6/CH_3CN at +25 °C versus ferrocene$^{+/0}$. [c] Comproportionation constant, K_c determined as $10^{(\Delta E_{ox}/0.059)}$ at +25 °C.[40]

systems have been completely assigned on the basis of comparisons with the electrochemical data,[38,39] and resonance Raman measurements.[24]

In the present report, minor differences were observed in the band energies and intensities between the diastereoiosmers of the partially- and fully-oxidised di- and trinuclear systems. The IVCT spectra for *meso*- and *rac*-[{Ru(bpy)$_2$}$_2$(μ-hat)]$^{5+}$ are shown in Figure 2a. Spectroelectrochemical generation of the mixed-valence +5, and fully-oxidised +6 forms of the dinuclear *meso*- and *rac*-[{Ru(bpy)$_2$}$_2$-

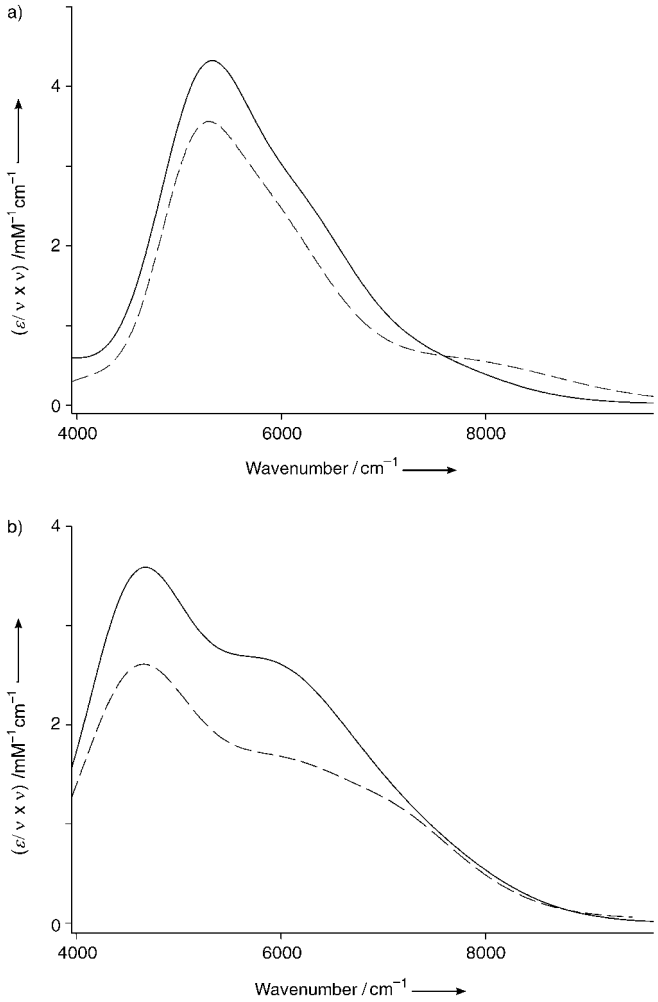

Figure 2. Near-infrared (NIR) spectra of the di- and trinuclear systems. a) Overlay of the IVCT bands for *meso*- (——) and *rac*- [{Ru(bpy)$_2$}$_2$(μ-hat)]$^{5+}$ (-----) at −35 °C {plotted as $(\varepsilon/\nu \times \nu)$ vs ν}. b) Overlay of the IVCT bands for heterochiral- (——) and homochiral [{Ru(bpy)$_2$}$_3$(μ-hat)]$^{7+}$ at −15 °C {plotted as $(\varepsilon/\nu \times \nu)$ vs ν}.

(μ-hat)]$^{n+}$ diastereoisomers at −35 °C revealed stable isosbestic points in the spectral progressions accompanying both oxidation processes. The ^{1}MLCT absorption bands decreased in intensity following one-electron oxidation and eventually collapsed on further oxidation to the +6 species. The formation of the fully-oxidised +6 species was characterised by the appearance of intense π*(bpy)→dπ(Ru^{III}) and π*(hat)→dπ(Ru^{III}) ligand-to-metal (LMCT) absorptions in the region 10000–16000 cm^{-1}. The energies of these bands are consistent with the previously assigned π*(bpy)→dπ(Ru^{III}) LMCT transitions at 14815 and 17160 cm^{-1} in [Ru^{III}(bpy)$_3$]$^{3+}$.[43] Spectral deconvolution was performed to reveal the behaviour of the underlying transitions responsible for the variation in the spectra with the extent of oxidation of the assembly.

The presence of the third {Ru(bpy)$_2$}$^{2+}$ moiety in the unoxidised +6 forms of the trinuclear systems has the effect of increasing the absorptivity, and shifting the ^{1}MLCT transition to lower energy relative to their dinuclear congeners. Masschelein and co-workers[38] have rationalised this observation on the basis of spectral-electrochemical correlations: the energy of the highest occupied dπ molecular orbital is relatively invariant to the addition of an {Ru(bpy)$_2$}$^{2+}$ moiety, whereas the lowest unoccupied π* molecular orbital is stabilised by the addition.

Spectroelectrochemical oxidation of the trinuclear complexes allowed the generation of the mixed-valence +7 and +8 forms, and fully-oxidised +9 forms at −15 °C (Figure 3). Stable isosbestic points were observed in the spectral progressions accompanying the three stages of oxidation. The ^{1}MLCT absorption bands decreased in intensity following one- and two-electron oxidation, and eventually collapsed completely on further oxidation to the +9 species.

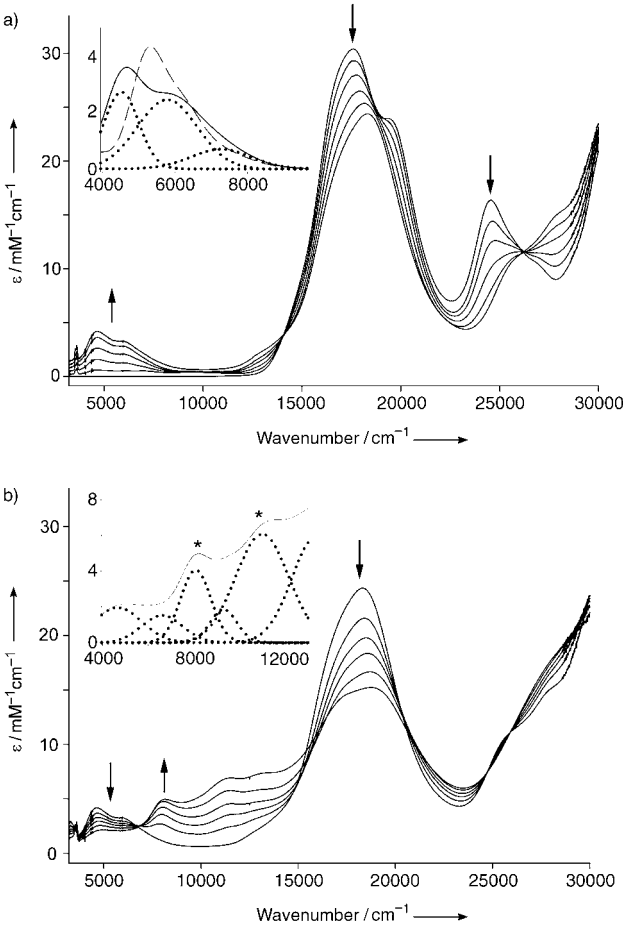

Figure 3. Spectroelectrochemistry for the oxidation of the trinuclear complex heterochiral-[{Ru(bpy)$_2$}$_3$(μ-hat)]$^{n+}$ (a) Spectroelectrochemical changes for the oxidation reaction heterochiral-[{Ru(bpy)$_2$}$_3$(μ-hat)]$^{6+}$→heterochiral-[{Ru(bpy)$_2$}$_3$(μ-hat)]$^{7+}$ at −15 °C. The inset shows IVCT bands {plotted as $(\varepsilon/\nu \times \nu)$ vs ν} for *meso*-[{Ru(bpy)$_2$}$_2$(μ-hat)]$^{5+}$ (-----) at −35 °C and heterochiral-[{Ru(bpy)$_2$}$_3$(μ-hat)]$^{7+}$ (——) at −15 °C in addition to the bands obtained from Gaussian deconvolution of the latter (•••••). b) Spectroelectrochemical changes for the oxidation reaction heterochiral-[{Ru(bpy)$_2$}$_3$(μ-hat)]$^{7+}$→heterochiral-[{Ru(bpy)$_2$}$_3$(μ-hat)]$^{8+}$ at −15 °C. The inset shows IVCT bands {plotted as $(\varepsilon/\nu \times \nu)$ vs ν} for heterochiral-[{Ru(bpy)$_2$}$_3$(μ-hat)]$^{8+}$ (——; maxima indicated by asterisks) at −15 °C in addition to the bands obtained from Gaussian deconvolution (•••••).

Oxidation of the formally Ru^{II} to Ru^{III} centres was accompanied by an increase in the intensity of the transitions in the region 10000–16000 cm^{-1}. These are assigned as ligand-to-metal $\pi^*(bpy)\rightarrow d\pi(Ru^{III})$ and $\pi^*(hat)\rightarrow d\pi(Ru^{III})$ LMCT transitions by comparison with the behaviour of the analogous mono- and dinuclear systems.

Intervalence charge transfer: The near-infrared (NIR) spectra of the di- and trinuclear systems spectra were scaled as $\Sigma\varepsilon(\nu)/\nu\, d\nu$[44,45] and deconvoluted by use of the software package GRAMS32. The results of the band maxima (ν_{max}), molar extinction coefficients (ε), and bandwidths ($\Delta\nu_{1/2}$) derived from the deconvolution procedure are summarised in Table 2.

Table 2. NIR spectral data of the reduced absorption spectra (ε/ν vs ν) for the di- and trinuclear complexes at −35 and −15 °C, respectively. For the dinuclear species, the parameters for the overall NIR band envelopes are shown in bold type: details of the deconvoluted bands are in normal type.

Complex	Component	$\nu_{max}\pm 10$ [cm^{-1}]	$\varepsilon_{max}\pm 0.01$ [$mM^{-1}cm^{-1}$]	$\Delta\nu_{1/2(exptl)}\pm 20$ [cm^{-1}]	$\Delta\nu^0_{1/2}$ [a] [cm^{-1}]
meso-$[\{Ru(bpy)_2\}_2(\mu\text{-hat})]^{5+}$		**5250**	**4.230**	**1600**	**3100**
		3870[c]	0.518	827	
	A	5150	3.245	1020	3075
	B	5950	2.040	1410	3305
	C	6985	0.565	2560	3580
rac-$[\{Ru(bpy)_2\}_2(\mu\text{-hat})]^{5+}$		**5240**	**3.540**	**1485**	**3100**
		4030[c]	0.193	708	
	A	5110	1.900	824	3065
	B	5710	2.450	1515	3240
	C	7615	0.454	2295	3740
heterochiral-$[\{Ru(bpy)_2\}_3(\mu\text{-hat})]^{7+}$	A	4515	3.185	1225	
	B	5820	2.300	1610	
	C	7160	0.889	1715	
heterochiral-$[\{Ru(bpy)_2\}_3(\mu\text{-hat})]^{8+}$[b]		4715	2.085	2735	
		6455	0.840	1260	
		7980*	4.510	1740	
		9350	2.040	1440	
		10900*	5.950	2515	
		13145	5.970	2445	
		14770	1.560	1725	
		16790	12.37	3735	
		19660	11.63	1655	
homochiral-$[\{Ru(bpy)_2\}_3(\mu\text{-hat})]^{7+}$	A	4475	2.150	1255	
	B	5750	1.430	1930	
	C	7180	0.757	1680	
homochiral-$[\{Ru(bpy)_2\}_3(\mu\text{-hat})]^{8+}$[b]		4460	1.825	1460	
		6745*	3.045	5670	
		11060*	2.750	2450	
		13270	6.000	2035	
		17890	21.90	5490	

[a] For weakly interacting (Class II) systems,[46] $\Delta\nu^0_{1/2}=[16kT\ln 2\ (\nu_{max})]^{1/2}$ where $16kT\ln 2 = 1836\ cm^{-1}$ at 238 K. [b] Band characteristics for the transitions of IVCT origin are indicated by asterisks. [c] Artifact peak at detector limit.

Dinuclear systems: The first oxidation process for the diastereoisomers of the dinuclear complex $[\{Ru(bpy)_2\}_2(\mu\text{-hat})]^{4+}$ was characterised by the appearance of an intense new band in the region 3500–8000 cm^{-1} {ε_{max}= 4230 (*meso*) and 3540 $M^{-1}cm^{-1}$ (*rac*)}, which collapsed completely on removal of the second electron: on this basis, the band was assigned as an IVCT transition (Table 2, Figure 2a). The bands appear asymmetrical and narrower on the lower energy side with bandwidths at half-height ($\Delta\nu_{1/2(exptl)}$) of 1600 (*meso*) and 1485 cm^{-1} (*rac*). Compared with the theoretical bandwidths ($\Delta\nu^0_{1/2}$) of 3100 cm^{-1} for both diastereoisomers, estimated on the basis of the classical two-state theory {Eq. (1), where $16RT\ln(2) = 1836\ cm^{-1}$ at 238 K and ν_{max} is the IVCT maximum of the reduced absorption spectrum},[46] the relatively narrow observed bandwidths point towards significant electronic communication between the metal centres.

$$\Delta\nu^0_{1/2} = [16RT\ln(2)\nu_{max}]^{1/2} \quad (1)$$

Within this classical treatment,[11] the parameter Γ provides a criterion for describing the degree of electronic coupling in the system:

$$\Gamma = 1-(\Delta\nu_{1/2(exptl)})/[16RT\ln(2)\nu_{max}]^{1/2} = 1-(\Delta\nu_{1/2(exptl)})/(\Delta\nu^0_{1/2}) \quad (2)$$

where $0 < \Gamma < 0.5$ for weak to moderate coupling (localised Class II systems), $\Gamma \approx 0.5$ at the Class II–III transition, and $\Gamma > 0.5$ for strongly coupled (delocalised Class III) systems. In the present case, Γ=0.484 (*meso*) and 0.521 (*rac*) which suggests that the systems lie close to the localised-delocalised transition, with the *rac* diastereoisomer exhibiting a marginally greater degree of electronic delocalisation relative to the *meso* form.

When $0 < \Gamma < 0.5$, the electron coupling parameter H_{ab} is given by[11]

$$H_{ab} = 2.06\times 10^{-2}\ (\nu_{max}\varepsilon_{max}\Delta\nu_{1/2(exptl)})^{1/2}/r_{ab} \quad (3)$$

where r_{ab} is the *effective* electron transfer distance, which can be obtained from measurements of the dipole moment change associated with the IVCT process through electroabsorption (Stark effect) spectroscopy.[47] In the absence of these measurements, however, r_{ab} is generally equated with the through-space geometrical distance between the metal centres.[10] Since this geometric distance is likely to be greater than the actual (*effective*) charge transfer distance due to electronic coupling across the bridge, Equation (3) provides

a lower limit only for H_{ab}. With this caveat noted, $H_{ab} = 584$ and 514 cm^{-1} for the *meso* and *rac* diastereoisomers, respectively, where r_{ab} is equated with the approximate geometric metal–metal separation of 6.65 Å.

The interpretation of the IVCT data for the dinuclear HAT-bridged systems is challenging because they appear to lie at transition between the localised and delocalised regimes, where classical models[11,44,48,49] break down due to the failure of the Born–Oppenheimer approximation upon which they are based.[10,11] The treatment of the full vibronic coupling problem[50–53] is central to the quantitative analysis of these borderline localised-to-delocalised systems; however, the application of such methods is beyond the scope of the present work. Instead, we seek to investigate the qualitative correspondence between the IVCT properties of the di- and trinuclear complexes on the basis of two alternate descriptions based on localised and delocalised models.

A localised model for IVCT: From a localised viewpoint, the asymmetric appearance of the IVCT bands is attributed to the "band cut-off" effect which occurs at $h\nu = 2H_{ab}$, and is more pronounced for systems lying closer to the localised-to-delocalised transition.[11,54,55] Alternatively, the asymmetry of the IVCT bands may be attributed to a manifold of discrete, underlying transitions which are identified as spin-orbit components.[10,56–58]

Spectral deconvolution of the reduced ($\Sigma\varepsilon(\nu)/\nu\ d\nu$) NIR bands reveals three underlying gaussian-shaped components (Table 2). The differences observed between the energies, intensities and bandwidths for the diastereoisomers lie well outside the limits of experimental error. The lowest energy components at 3870 and 4030 cm^{-1} in the *meso* and *rac* diastereoisomers of the dinuclear complex, respectively, appear to be artifacts which arise near the limit of the NIR spectrometer at ~3000 cm^{-1}. For both diastereoisomers, components A and B dominate the IVCT manifolds, although the integrated intensities differ between the two forms: component A dominates B for the *meso* form (i.e., A:B 1.35:1), while the opposite is observed for the *rac* form (i.e., B:A 2.25:1). For the overall IVCT manifolds, the integrated intensity for the *meso* diastereoisomer is greater than that for the *rac* form, and suggests a greater degree of metal–metal interaction in the former. This contradicts the previous assessment of the relative extent of metal–metal coupling on the Γ parameter, where the coupling was greater in the *rac* diastereoisomer. Since the integrated intensity of the IVCT manifold (i.e., the band area) is directly proportional to the extent of delocalisation in the mixed-valence ground state,[46] these values are expected to provide a more accurate estimate of delocalisation in the diastereoisomeric forms rather than the Γ parameter which is based on bandwidth measurements alone.

The intervalence process occurs through an electron transfer superexchange mechanism via the π and π^* orbitals of the bridging ligand. Based on the coordinate designation in Figure 4, qualitative considerations indicate that the metal-based orbitals with z character are appropriate for overlap

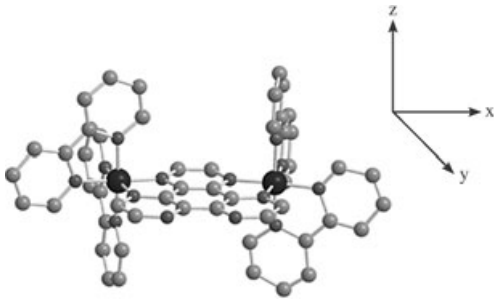

Figure 4. Coordinate axes for the *rac* ($\Delta\Delta$) diastereoisomer of $[\{Ru(bpy)_2\}_2(\mu\text{-hat})]^{4+}$. Hydrogen atoms are omitted for clarity.

with the π,π^*(hat) system and will be stabilised to a relatively greater extent (and will thus lie lower in energy) than those that lie orthogonal to the π,π^*(hat) system; that is, the d_{xy} orbitals that lie in the plane of the bridging ligand. In order of increasing energy, the three $d\pi$ orbitals may be more closely represented by d_{xz},d_{yz}($d\pi_1$,$d\pi_2$) and d_{xy}($d\pi_3$).

Intervalence charge transfer can arise due to separate electronic excitations from any $d\pi_n$ orbital at Ru^{II} to the hole in the corresponding $d\pi_n$ orbital which is present in any of the three spin-orbit states at Ru^{III} (Figure 5).[10] These transitions are identified with the three underlying components in the IVCT band, separated by the energy differences between the ground and two excited spin-orbit states, $\Delta E_{so(1)}$ and $\Delta E_{so(2)}$:

$$\Delta E_{so(1)} \approx \nu_{max}\{IVCT(B)\} - \nu_{max}\{IVCT(A)\} \quad (4a)$$

$$\Delta E_{so(2)} \approx \nu_{max}\{IVCT(C)\} - \nu_{max}\{IVCT(A)\} \quad (4b)$$

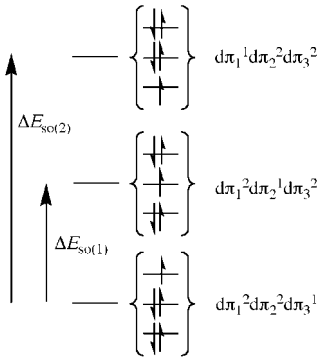

Figure 5. Schematic energy level diagram showing the relative energies of the spin-orbit levels.

The energy separation between the first and second, and second and third components of the IVCT bands (Table 2) are approximated by $\Delta E_{so(1)}$ and $\Delta E_{so(2)}$, which are, respectively, 800 and 1035 cm^{-1} for the *meso* form, and 600 and 1905 cm^{-1} for the *rac* form. The energy splittings between the underlying components are within the range expected for spin-orbit coupling between Ru^{II} and Ru^{III} centres (i.e., ~800–1250 cm^{-1}) for the *meso* diastereoisomer, although for

the *rac* form the splitting between IVCT(B) and IVCT(C) is significantly greater than expected. The differences between the diastereoisomers indicate that stereochemical factors such as different solvent and anion interactions with the forms may also influence the inter-metal electronic interaction.[36] For IVCT(A), ν_{max} is comparable for the two diastereoisomers {5150 and 5110 cm^{-1} for the *meso* and *rac* forms, respectively}; however, H_{ab} for the *meso* form is considerably greater than that for the *rac* form {405 vs 275 cm^{-1}}.

The intensities of the three IVCT components should be proportional to the degree of orbital overlap between the dπ orbitals at the formally Ru^{II} centre and the dπ orbital containing the hole at the formally Ru^{III} centre. The integrated intensities and H_{ab} values provide an indication of inherent differences in the extent of orbital overlap between the donor and acceptor orbitals in the diastereoisomeric forms.

For both diastereoisomers, IVCT(C) has the lowest intensity: this component can be assigned as a $(Ru^{II})d\pi_3$–π*-(hat)–$(Ru^{III})d\pi_3$ transition {abbreviated $d\pi_3$–π*(hat)–$d\pi_3$}; it is broad and has low absorptivity as the electronic coupling occurs between the donor and acceptor orbitals which are *predominantly* d_{xy} in character, and thus oriented orthogonal to the π,π*(hat) system.

For the *rac* form, the integrated intensities of the IVCT components reveal that component B dominates the IVCT manifold (i.e., the ratio of the intensities is given by B:A 2.25:1), while component A is dominant for the *meso* form (i.e., A:B 1.35:1). Based on ligand field considerations, IVCT(A) and (B) are associated with $d\pi_1$–π*(hat)–$d\pi_1$ and $d\pi_2$–π*(hat)–$d\pi_2$ interactions across the bridge, where $d\pi_1$ and $d\pi_2$ are predominantly d_{xz} and d_{yz} in character. The enhanced $d\pi_2$–π*(hat)–$d\pi_2$ interaction relative to the $d\pi_1$–π*-(hat)–$d\pi_1$ interaction in the *rac* form suggests that the $d\pi_2$ orbitals of the formally Ru^{II} (donor) and Ru^{III} (acceptor) centres are overlapped more effectively when the stereochemistries of the two metal centres are equivalent. This trend in the relative intensities of the IVCT components has been observed for the diastereoisomeric forms of a range of dinuclear complexes which incorporate angular-bridging ligands; that is, where the bidentate binding sites of the bridging ligands are angularly disposed.[59]

A delocalised model for IVCT: The bridging HAT ligand plays an integral role in mediating the intervalence electron transfer process between the metal centres via a superexchange-assisted mechanism.[60] This suggests that the explicit inclusion of a third electronic state associated with the bridging ligand may be required to rationalise the underlying electronic structure of the IVCT bands. In this case, the IVCT transition is described as delocalised, and the transition is due to electron transfer between the bonding and non-bonding molecular orbitals within the molecular orbital manifold of the system (Figure 6).[61–67] The components of the band arise from the combined effects of spin-orbit coupling and lower symmetry perturbations and their relative intensities are determined by the extent of orbital overlap between the donor and acceptor orbitals, and the position of the hole in the latter.

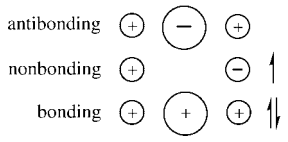

Figure 6. Qualitative molecular orbital diagram for the dinuclear $[\{Ru(bpy)_2\}_2(\mu\text{-hat})]^{5+}$ system showing the bonding, non-bonding and antibonding molecular orbitals. The IVCT corresponds to a bonding→nonbonding transition.

Trinuclear systems: The two mixed-valence states of the trinuclear diastereoisomers were realised upon one- and two-electron oxidation of the +6 species at −15 °C. The NIR spectra of the +7 and +8 mixed-valence forms (Figures 2b and 3) exhibit striking differences from one another (which lie well outside the limits of experimental error), and from their dinuclear analogues.

The generation of the +7 mixed-valence species for both diastereoisomers was accompanied by the appearance of new absorption bands in the range 3500–9000 cm^{-1} (Figures 2b and 3a, Table 2). Spectral deconvolution revealed the presence of three underlying transitions, separated by 1305 and 1340 cm^{-1} (heterochiral) and 1275 and 1430 cm^{-1} (homochiral). The integrated intensities of the components indicate that the transitions denoted A and B dominate the IVCT manifold (i.e., A > B > C), with ratios of 3.87:2.84:1 (heterochiral) and 2.81:2.48:1 (homochiral). This relative energy ordering differs from that found for the dinuclear diastereoisomers where IVCT(B) was found to dominate the IVCT manifold. The overall integrated intensity of the IVCT manifold for the heterochiral form is slightly greater than that for the homochiral form, and the intensities are approximately twice those for the related dinuclear complexes. The difference may be rationalised on the basis of the doubly-degenerate nature of the optically-induced transition from the two formally Ru^{II} centres to the hole at the formally Ru^{III} centre in the trinuclear species. It should be noted that the comparison between the di- and trinuclear cases may not be strictly valid due to the different temperatures at which the experiments were conducted.

Components B and C exhibit comparable energies and separations relative to the same components in the dinuclear diastereoisomers, although component A is significantly red-shifted (by ~600 cm^{-1}) relative to the same component in the dinuclear systems.

While vibronic coupling models may provide a more quantitative understanding of the NIR bands, the magnitude of the splitting observed between the two dominant underlying transitions in the NIR band manifold is still consistent with a localised description. On this basis, the bands are assigned as separate optically-induced transitions between energy levels within the molecular orbital manifold of the trinuclear complexes which are split predominantly by spin-orbit coupling of the metal centres. Relative to the dinuclear

diastereoisomers, component A experiences the most pronounced energy shift, while components B and C appear relatively unperturbed.

Based on the coordinate description invoked for the dinuclear complex (Figure 4), it would appear that the incorporation of a third $\{Ru(bpy)_2\}^{2+}$ moiety will perturb the dπ orbitals oriented towards the additional Ru centre to the greatest extent. Since electronic delocalisation within the assembly is governed by superexchange coupling through the π* orbitals of the bridging ligand, the orbitals perturbed most significantly are predominantly d_{xz} and d_{yz} in character, and have already been assigned as the dominant Cartesian components of $d\pi_1$ and $d\pi_2$ for the dinuclear complexes.

On inclusion of the third chromophore, the orbital overlap of the d_{xz},d_{yz}($d\pi_1$,$d\pi_2$) orbitals at the two formally Ru^{II} centres with the hole at the formally Ru^{III} centre should be equivalent since they are equidistant to the acceptor. This contrasts the situation in the dinuclear system, where greater overlap is expected for the orbitals directed towards the Ru^{II} centre compared with those directed towards the vacant coordination site. Based on this localised argument, component A in the trinuclear complex—which is the component shifted most significantly relative to the dinuclear diastereoisomers—would involve optically-induced electron transfer between molecular orbitals centred over the core of the bridging HAT ligand. Accordingly, components A, B and C represent, respectively, IVCT transitions which originate from $d\pi_1$–π*(hat)–$d\pi_1$, $d\pi_2$–π*(hat)–$d\pi_2$ and $d\pi_3$–π*(hat)–$d\pi_3$ interactions across the bridge, where $d\pi_1$ and $d\pi_2$ are predominantly d_{xz} and d_{yz}, and $d\pi_3$ is predominantly d_{xy} in character. As was the situation with the dinuclear forms, the low intensity of the $d\pi_3$–π*(hat)–$d\pi_3$ interaction is consistent with the orthogonal orientation of the d_{xy}($d\pi_3$) orbitals relative to the π,π*(hat) orbtials.

On the basis of a localised analysis for the spectral properties of the +5 forms of the dinuclear mixed-valence complexes, and +7 forms of the trinuclear systems, the presence of a third $\{Ru(bpy)_2\}^{2+}$ chromophore in the trinuclear assembly amplifies the energy splitting between the spin-orbit coupling states, and leads to a two-fold enhancement in the electronic interaction mediated by HAT. It is interesting to consider this result in light of previous IVCT measurements on the mixed-valence forms of the trinuclear CN^--bridged chain $[NC\text{-}Ru^{II}(bpy)_2\text{-}CN\text{-}Ru^{III}(bpy)_2\text{-}NC\text{-}Ru^{II}(bpy)_2\text{-}CN]^{3+}$.[68–71] The NIR region of the mixed-valence species exhibited a broad band (assigned as an IVCT transition) in the region 4500–12000 cm^{-1} which appeared to comprise of two underlying components of approximately equal intensity. By comparison, the analogous dinuclear complex $[NC\text{-}Ru^{II}(bpy)_2\text{-}CN\text{-}Ru^{III}(bpy)_2\text{-}CN]^{2+}$ revealed a single absorption band at 5700 cm^{-1}. The apparent splitting of the IVCT transition into two components in the trinuclear case was attributed to non-negligible superexchange-assisted through-bond coupling between the *remote* metal centres, and the result was rationalised by the construction of adiabatic energy surfaces for the trinuclear system.[68–71] For the HAT-bridged systems in the present study, the three metal centres share the same bridging ligand, and are equivalently disposed from one another, such that a *remote* superexchange mechanism cannot be invoked.

The intensity of the bands decreased on subsequent oxidation to the +8 mixed-valence species, with the appearance of new bands at ~8000 and 11500 cm^{-1} (Figure 3b; Table 2). The transitions in the region at higher energies than 13000 cm^{-1} were assigned as ligand-to-metal (LMCT) and metal-to-ligand (MLCT) absorptions by comparison with the related dinuclear species, and by their behaviour on oxidation to the +9 species. Assignment of the bands in the region at energies lower than 7000 cm^{-1} is ambiguous due to the presence of complicating comproportionation equilibria, although these may be reasonably ascribed to the residual absorptions of the mono-oxidised +7 species. For the heterochiral diastereoisomer, the new absorption bands at ~8000 and 11500 cm^{-1}, which are solely characteristic of the +8 mixed-valence form, are assigned as IVCT transitions (Figure 2b). These transitions are expected to occur at higher energy than those in the +7 mixed-valence form due to the decreased electron delocalisation in the system, and hence destabilisation of the acceptor Ru^{III} orbitals. Accordingly, the predicted blue-shift in the energies of the absorption bands is observed, and is consistent with previous literature reports for IVCT transitions in related di- and trinuclear systems.[72] The ~3000 cm^{-1} separation between the bands assigned as IVCT transitions is not consistent with their interpretation based on spin-orbit coupling components however, and indicates that a molecular orbital approach—which includes vibronic coupling—may be essential.

The possibility also exists that the multiple IVCT transitions originate from optically-induced electron transfer between different "exciton" states. The doubly-oxidised (+8) species comprises two formally Ru^{III} and one formally Ru^{II} centre and therefore possesses two unpaired electrons. These may be aligned in a parallel or antiparallel fashion, giving rise to an overall singlet or triplet state for the trinuclear complex. The energy required for optical excitation to these two different "exciton" states will differ, in which case the two new transitions observed in the NIR region for the +8 species may be assigned as transitions to singlet and triplet exciton states in a valence-delocalised trinuclear mixed-valence species. A similar interpretation was proposed by Weyland et al.[73] to account for the observation of multiple IVCT transitions in valence-localised trinuclear complexes.

Conclusion

The IVCT properties of the mixed-valence forms of the diastereoisomers (*meso* and *rac*) of the dinuclear complex $[\{Ru(bpy)_2\}_2(\mu\text{-hat})]^{4+}$, and of the trinuclear species $[\{Ru(bpy)_2\}_3(\mu\text{-hat})]^{6+}$ (homochiral and heterochiral), display a marked dependence on the nuclearity and extent of oxidation of the mixed-valence assemblies, while small differences are also observed for the diastereoisomers of the same complex. The significant differences in IVCT properties between the di-

and trinuclear species are attributed to the extensive electronic communication between the $\{Ru(bpy)_2\}^{2+}$ chromophores, which gives rise to novel properties of the two mixed-valence states in the trinuclear case. The splitting of the IVCT transitions in the +7 species is attributed to the influence of spin-orbit coupling, while the two new dominant transitions in the NIR spectra of the +8 (diradical) species may arise from to transitions to separate *delocalised* exciton states of singlet and triplet character.

Alternative localised and delocalised approaches are discussed for the interpretation of the mixed-valence characteristics of the dinuclear systems, however treatment of the full vibronic coupling problem is necessary in order to provide a quantitative analysis of these borderline localised-to-delocalised systems. Qualitatively, a localised description based on the geometrical properties of the $d\pi(Ru^{II/III})$ orbitals provides a reasonable rationale for the IVCT behaviour in the di- and trinuclear systems.

The existence of quality experimental data that will test and guide developments in the conceptual theories for IVCT in higher nuclearity systems, and the extension of the IVCT probe to stereochemically unambiguous trinuclear species which exhibit strong electronic delocalisation, are extremely significant to our understanding of fundamental intramolecular electron transfer phenomena in polymetallic assemblies.

Experimental Section

Electrochemistry: Electrochemical measurements were performed under argon using a Bioanalytical Systems (BAS) 100 A Electrochemical Analyser. Cyclic (CV) and differential pulse (DPV) voltammograms were recorded in a standard three-electrode cell by using a glassy carbon or platinum button working electrode, a platinum wire auxiliary electrode and an Ag/AgCl reference electrode (0.1 mol dm^{-3} $[(n\text{-}C_4H_9)_4N]PF_6$ in CH_3CN). Ferrocene was added as an internal standard on completion of each experiment {the ferrocene/ferrocenium couple ($[FeCp_2]^{0/+}$) occurred at +550 mV versus Ag/AgCl}. Solutions contained 0.1 mol dm^{-3} $[(n\text{-}C_4H_9)_4N]PF_6$ as electrolyte. Cyclic voltammetry was performed with a sweep rate of 100 mV s^{-1}; differential pulse voltammetry was conducted with a sweep rate of 4 mV s^{-1} and a pulse amplitude, width and period of 50 mV, 60 ms and 1 s, respectively.

Spectroelectrochemistry: UV/visible/near-infrared (NIR) spectroelectrochemistry was performed using a CARY 5E spectrophotometer interfaced to Varian WinUV software. The absorption spectra of the electrogenerated mixed-valence species were obtained in situ by the use of a cryostatted Optically Semi-Transparent Thin-Layer Electrosynthetic (OSTLE) cell, path length 0.605 mm, mounted in the path of the spectrophotometer.[74]

Solutions for the spectroelectrochemial experiments contained 0.1 mol dm^{-3} $[(n\text{-}C_4H_9)_4N]PF_6$ supporting electrolyte in CH_3CN and the complex (ca. 1×10^{-3} mol dm^{-3}). All solutions were purged with N_2 prior to transference (via syringe) into the OSTLE cell. The temperature was stabilised to ± 0.3 °C prior to commencing electrolysis. The dinuclear systems required approximately 6 h for data collection at −35 °C, while the trinuclear systems required approximately 10 h and were conducted at −15 °C due to limitations on the extended supply of coolant gas.

Appropriate potentials were applied by using a BAS CV27 Voltammograph coupled to a digital LCD multimeter to permit careful control of both the current and potential during electrolysis. By this method, the electrogenerated species (which are otherwise unstable) were obtained in situ, and their absorption spectra recorded at regular intervals throughout the electrolysis. The attainment of a steady-state spectrum and the decay of the current to a constant minimum at a potential appropriately beyond $E_{1/2}$ (for the redox process in question) were indicative of the complete conversion of the starting material. For the mixed-valence species, a potential intermediate between the two metal-centred oxidation processes was employed. The reversibility of the spectral data was confirmed by the observation of stable isosbestic points, and the regeneration of the starting spectrum following the attainment of the steady-state spectrum for each mixed-valence species. For the systems under investigation in the present study which possess multiple redox processes, this procedure was repeated for each step before continuing to subsequent processes.

The IVCT spectra were scaled as $\Sigma\varepsilon(\nu)/\nu\ d\nu$.[44,45] An additional correction due to comproportionation of the mixed-valence species[75] was not applied since the proportion of the complex in the mixed-valence form (at equilibrium) was > 97.5 %, and the correction does not influence the conclusions reached regarding the relative electronic coupling in the systems investigated. To minimise artefacts in the NIR spectral data due to ion-pairing and concentration effect which are known to influence the IVCT transitions of dinuclear complexes,[36,76–79] the spectra were measured using a constant concentration of complex (ca. 1×10^{-3} mol dm^{-3}) under identical conditions of electrolyte {0.1 mol dm^{-3} $[(n\text{-}C_4H_9)_4N]PF_6$} and temperature.

Spectral deconvolution: Spectral deconvolution of the near-infrared transitions was performed using the curve-fitting subroutine implemented within the GRAMS32 commercial software package. For the dinuclear complexes, convergence of the iteration procedure was achieved for three Gaussian-shaped bands under the IVCT manifold. The characteristics of the components were found to vary slightly over repeat iterations, however the relative energies, intensities and bandwidths of the transitions remained constant. The band characteristics are presented as an average of the solutions for the repeat iterations. Based on the reproducibility of the parameters obtained from the deconvolutions, the uncertainties in the energies (ν), intensities (ε) and bandwidths ($\Delta\nu_{1/2}$) were estimated as ±10 cm^{-1}, ±10 M^{-1} cm^{-1} and ±20 cm^{-1}, respectively.

Materials: Acetonitrile (CH_3CN; Aldrich, 99.9+ %) was distilled under nitrogen from CaH_2 immediately prior to use. $[(n\text{-}C_4H_9)_4N]PF_6$ (Fluka; puriss. electrochemical grade) was dried under vacuum at 45 °C before use.

Complex syntheses and diastereoisomer separation: The syntheses and characterisation of $[\{Ru(bpy)_2\}_2(\mu\text{-hat})](PF_6)_4$ and $[\{Ru(bpy)_2\}_3(\mu\text{-hat})](PF_6)_6$, as well as the separation and purification of the respective diastereoisomers, were performed using the techniques reported previously.[16]

Acknowledgements

This work was supported by the Australian Research Council. We also thank Dr. Jeff Reimers (University of Sydney) for invaluable discussions on various aspects of analysis of the data.

[1] V. Balzani, L. De Cola, *Supramolecular Chemistry*, *Vol. 371*, Kluwer Academic, Dordrecht, **1992**.
[2] J.-M. Lehn, *Supramolecular Chemistry*, VCH, Darmstadt, **1995**.
[3] J.-P. Sauvage, M. W. Hosseini, *Comprehensive Supramolecular Chemistry*, *Vol. 9*, Pergamon, Oxford, **1996**.
[4] C. Provent, A. F. Williams, in *Transition Metals in Supramolecular Chemistry* (Ed.: J. P. Sauvage), Wiley, Chichester, **1999**, pp. 135.
[5] J. W. Steed, J. L. Atwood, *Supramolecular Chemistry*, Wiley, Chichester, **2000**.
[6] P. D. Beer, D. K. Smith, in *Progress in Inorganic Chemistry*, *Vol. 46* (Ed.: K. D. Karlin), Wiley, New York, **1997**, pp. 1.
[7] V. Balzani, A. Juris, M. Venturi, S. Campagna, S. Serroni, *Chem. Rev.* **1996**, *96*, 759.

[8] V. Balzani, S. Campagna, G. Denti, A. Juris, S. Serroni, M. Venturi, *Solar Energy Materials Solar Cells* **1995**, *38*, 159.
[9] C. A. Bignozzi, J. R. Schoonover, F. Scandola, in *Progress in Inorganic Chemistry, Vol. 44* (Ed.: G. J. Meyer), Wiley, New York, **1997**, p. 1.
[10] K. D. Demadis, C. M. Hartshorn, T. J. Meyer, *Chem. Rev.* **2001**, *101*, 2655.
[11] B. S. Brunschwig, C. Creutz, N. Sutin, *Chem. Soc. Rev.* **2002**, *31*, 168.
[12] M. J. Powers, R. W. Callahan, D. J. Salmon, T. J. Meyer, *Inorg. Chem.* **1976**, *15*, 894.
[13] A. von Kameke, G. M. Tom, H. Taube, *Inorg. Chem.* **1978**, *17*, 1790.
[14] F. R. Keene, *Coord. Chem. Rev.* **1997**, *166*, 122.
[15] F. R. Keene, *Chem. Soc. Rev.* **1998**, *27*, 185.
[16] T. J. Rutherford, O. Van Gijte, A. Kirsch-De Mesmaeker, F. R. Keene, *Inorg. Chem.* **1997**, *36*, 4465.
[17] T. J. Rutherford, F. R. Keene, *Inorg. Chem.* **1997**, *36*, 3580.
[18] T. J. Rutherford, P. A. Pellegrini, J. Aldrich-Wright, P. C. Junk, F. R. Keene, *Eur. J. Inorg. Chem.* **1998**, 1677.
[19] T. Okubo, S. Kitagawa, M. Kondo, H. Matsuzaka, T. Ishii, *Angew. Chem.* **1999**, *111*, 190; *Angew. Chem. Int. Ed.* **1999**, *38*, 931; .
[20] C. Moucheron, A. Kirsch-De Mesmaeker, S. Choua, *Inorg. Chem.* **1997**, *36*, 584.
[21] I. Ortmans, P. Didier, A. Kirsch-de Mesmaeker, *Inorg. Chem.* **1995**, *34*, 3695.
[22] P. Didier, I. Ortmans, A. Kirsch-De Mesmaeker, R. J. Watts, *Inorg. Chem.* **1993**, *32*, 5239.
[23] R. Sahai, D. P. Rillema, R. Shaver, S. Van Wellendael, D. C. Jackman, M. Boldaji, *Inorg. Chem.* **1989**, *28*, 1022.
[24] A. Kirsch-De Mesmaeker, L. Jacquet, A. Masschelein, F. Vanhecke, K. Heremans, *Inorg. Chem.* **1989**, *28*, 2465.
[25] P. N. W. Baxter, J.-M. Lehn, B. O. Kneisel, G. Baum, D. Fenske, *Chem. Eur. J.* **1999**, *5*, 113.
[26] J.-P. Lecomte, A. K.-D. Mesmaeker, M. M. Feeney, J. M. Kelly, *Inorg. Chem.* **1995**, *34*, 6481.
[27] J. R. Galán-Mascarós, K. R. Dunbar, *Chem. Commun.* **2001**, 217.
[28] H. Grove, J. Sletten, M. Julve, F. Lloret, J. Cano, *J. Chem. Soc. Dalton Trans.* **2001**, 259.
[29] S. R. Marshall, A. L. Rheingold, L. N. Dawe, W. W. Shum, C. Kitamura, J. Miller, *Inorg. Chem.* **2002**, *41*, 3599.
[30] B. F. Abrahams, P. A. Jackson, R. Robson, *Angew. Chem.* **1998**, *110*, 2801; *Angew. Chem. Int. Ed.* **1998**, *37*, 2656.
[31] S. Masaoka, S. Furukawa, H.-C. Chang, T. Mizutani, S. Kitagawa, *Angew. Chem.* **2001**, *113*, 3933; *Angew. Chem. Int. Ed.* **2001**, *40*, 3817.
[32] V. Balzani, F. Scandola, *Supramolecular Photochemistry*, Ellis Horwood, Chichester, **1991**.
[33] L. S. Kelso, D. A. Reitsma, F. R. Keene, *Inorg. Chem.* **1996**, *35*, 5144.
[34] T. J. Rutherford, F. R. Keene, *Inorg. Chem.* **1997**, *36*, 2872.
[35] J. A. Treadway, P. Chen, T. J. Rutherford, F. R. Keene, T. J. Meyer, *J. Phys. Chem. A* **1997**, *101*, 6824.
[36] D. M. D′Alessandro, L. S. Kelso, F. R. Keene, *Inorg. Chem.* **2001**, *40*, 6841.
[37] T. J. Rutherford, F. R. Keene, *J. Chem. Soc. Dalton Trans.* **1998**, 1155.
[38] A. Masschelein, A. Kirsch-De Mesmaeker, C. Verhoeven, R. Nasielski-Hinkens, *Inorg. Chim. Acta* **1987**, *129*, L13.
[39] L. Jacquet, A. Kirsch-De Mesmaeker, *J. Chem. Soc. Faraday Trans.* **1992**, *88*, 2471.
[40] C. Creutz, *Prog. Inorg. Chem.* **1983**, *30*, 1.
[41] R. J. Crutchley, *Adv. Inorg. Chem.* **1994**, *41*, 273.
[42] D. E. Richardson, H. Taube, *Coord. Chem. Rev.* **1984**, *60*, 107.
[43] K. Kalyanasundaram, S. M. Zakeeruddin, M. K. Nazeeruddin, *Coord. Chem. Rev.* **1994**, *132*, 259.
[44] N. S. Hush, *Prog. Inorg. Chem.* **1967**, *8*, 391.
[45] J. R. Reimers, N. S. Hush, *Inorg. Chem.* **1990**, *29*, 3686.
[46] N. S. Hush, *Coord. Chem. Rev.* **1985**, *64*, 135.
[47] G. U. Bublitz, S. G. Boxer, *Annu. Rev. Phys. Chem.* **1997**, *48*, 213.
[48] N. S. Hush, *Electrochim. Acta* **1968**, *13*, 1005.
[49] B. S. Brunschwig, N. Sutin, *Coord. Chem. Rev.* **1999**, *187*, 233.
[50] S. B. Piepho, E. R. Krausz, P. N. Schatz, *J. Am. Chem. Soc.* **1978**, *100*, 2996.
[51] S. B. Piepho, *J. Am. Chem. Soc.* **1988**, *110*, 6319.
[52] K. Y. Wong, P. N. Schatz, *Prog. Inorg. Chem.* **1981**, *28*, 369.
[53] J. R. Reimers, N. S. Hush, *Chem. Phys.* **1996**, *208*, 177.
[54] S. F. Nelsen, *Chem. Eur. J.* **2000**, *6*, 581.
[55] C. Lambert, G. Nöll, *J. Am. Chem. Soc.* **1999**, *121*, 8434.
[56] K. D. Demadis, E.-S. El-Samanody, G. M. Coia, T. J. Meyer, *J. Am. Chem. Soc.* **1999**, *121*, 535.
[57] K. D. Demadis, G. A. Neyhart, E. M. Kober, P. S. White, T. J. Meyer, *Inorg. Chem.* **1999**, *38*, 5948.
[58] G. A. Neyhart, C. J. Timpson, W. D. Bates, T. J. Meyer, *J. Am. Chem. Soc.* **1996**, *118*, 3730.
[59] D. M. D'Alessandro, F. R. Keene, unpublished results.
[60] G. Giuffrida, S. Campagna, *Coord. Chem. Rev.* **1994**, *135*, 517.
[61] L.-T. Zhang, J. Ko, M. J. Ondrechen, *J. Phys. Chem.* **1989**, *93*, 3030.
[62] L. J. Root, M. J. Ondrechen, *Chem. Phys. Lett.* **1982**, *93*, 421.
[63] J. Ko, M. J. Ondrechen, *Chem. Phys. Lett.* **1984**, *112*, 507.
[64] M. J. Ondrechen, J. Ko, L. J. Root, *J. Phys. Chem.* **1984**, *88*, 5919.
[65] J. Ko, M. J. Ondrechen, *J. Am. Chem. Soc.* **1985**, *107*, 6161.
[66] M. J. Ondrechen, J. Ko, L.-T. Zhang, *J. Am. Chem. Soc.* **1987**, *109*, 1672.
[67] L.-T. Zhang, J. Ko, M. J. Ondrechen, *J. Am. Chem. Soc.* **1987**, *109*, 1666.
[68] F. Scandola, R. Argazzi, C. A. Bignozzi, C. Chiorboli, M. T. Indelli, M. A. Rampi, *Coord. Chem. Rev.* **1993**, *125*, 283.
[69] C. A. Bignozzi, R. Argazzi, C. Chiorboli, F. Scandola, R. B. Dyer, J. R. Schoonover, T. J. Meyer, *Inorg. Chem.* **1994**, *33*, 1652.
[70] C. A. Bignozzi, S. Roffia, C. Chiorboli, J. Davila, M. T. Indelli, F. Scandola, *Inorg. Chem.* **1989**, *28*, 4350.
[71] C. A. Bignozzi, R. Argazzi, J. R. Schoonover, K. C. Gordon, R. B. Dyer, F. Scandola, *Inorg. Chem.* **1992**, *31*, 5260.
[72] B. W. Pfennig, J. L. Cohen, I. Sosnowski, N. M. Novotny, D. M. Ho, *Inorg. Chem.* **1999**, *38*, 606.
[73] T. Weyland, K. Costuas, L. Toupet, J.-F. Halet, C. Lapinte, *Organometallics* **2000**, *19*, 4228.
[74] C. M. Duff, G. A. Heath, *Inorg. Chem.* **1991**, *30*, 2528.
[75] J.-P. Launay, *Chem. Soc. Rev.* **2001**, *30*, 386.
[76] M. D. Lowery, W. S. Hammack, H. G. Drickamer, D. N. Hendrickson, *J. Am. Chem. Soc.* **1987**, *109*, 8019.
[77] N. A. Lewis, Y. S. Obeng, *J. Am. Chem. Soc.* **1988**, *110*, 2306.
[78] N. A. Lewis, Y. S. Obeng, W. L. Purcell, *Inorg. Chem.* **1989**, *28*, 3796.
[79] R. L. Blackbourn, J. T. Hupp, *J. Phys. Chem.* **1990**, *94*, 1788.

Received: October 13, 2004
Published online: April 5, 2005